CORA Cork Open Research Archive
Cartlann Taighde Oscailte Chorcaí

Title	Quantification of black carbon mixing state from traffic: Implications for aerosol optical properties
Authors	Willis, Megan D.;Healy, Robert M.;Riemer, Nicole;West, Matthew;Wang, Jon M.;Jeong, Cheol-Heon;Wenger, John C.;Evans, Greg J.;Abbatt, Jonathan P. D.;Lee, Alex K. Y.
Publication date	2016-04-14
Original Citation	Willis, M. D., Healy, R. M., Riemer, N., West, M., Wang, J. M., Jeong, C. H., Wenger, J. C., Evans, G. J., Abbatt, J. P. D. and Lee, A. K. Y. (2016) 'Quantification of black carbon mixing state from traffic: implications for aerosol optical properties',Atmospheric Chemistry and Physics, 16, pp.4693-4706. doi: 10.5194/acp-16-4693-2016
Type of publication	Article (peer-reviewed)
Link to publisher's version	http://www.atmos-chem-phys.net/16/4693/2016/ - 10.5194/acp-16-4693-2016
Rights	© 2016, the Author(s). This work is distributed under the Creative Commons Attribution 3.0 License. - https://creativecommons.org/licenses/by/3.0/
Download date	2026-11-14 23:46:27
Item downloaded from	https://hdl.handle.net/10468/4179

UCC
University College Cork, Ireland
Coláiste na hOllscoile Corcaigh

Supplement of Atmos. Chem. Phys., 16, 4693–4706, 2016
http://www.atmos-chem-phys.net/16/4693/2016/
doi:10.5194/acp-16-4693-2016-supplement
© Author(s) 2016. CC Attribution 3.0 License.



Atmospheric Chemistry and Physics Open Access EGU

Supplement of

Quantification of black carbon mixing state from traffic: implications for aerosol optical properties

Megan D. Willis et al.

Correspondence to: Megan D. Willis (megan.willis@mail.utoronto.ca) and Alex K. Y. Lee (alexky.lee@utoronto.ca)

The copyright of individual parts of the supplement might differ from the CC-BY 3.0 licence.

S1 SP-AMS measurements of rBC and non-refractory aerosol species

The SP-AMS was calibrated for refractory black carbon (rBC) quantification using size-selected (300 nm), dried Regal Black (Regal 400R Pigment, Cabot Corp.) particles to determine the mass based ionization efficiency of rBC (mIE_{rBC}) (Onasch et al., 2012; Willis et al., 2014). The relative ionization efficiency for rBC ($RIE_{rBC} = mIE_{rBC}/mIE_{NO_3}$) was 0.2±0.05 ($1\sigma$ uncertainty), as experimentally determined before removal of the tungsten vaporizer. Assuming that RIE_{rBC} is constant, IE_{NO_3} was calculated based on measured values of mIE_{rBC} and known RIE_{rBC}. The average mIE_{rBC} was 189±20 ions/pg (for four independent calibrations throughout the study). Calculated IE_{NO_3} was then used with recommended relative ionization efficiencies (RIE) to quantify other, non-refractory, aerosol species associated with rBC (referred to as $NR\text{-}PM_{rBC}$) (Jimenez et al., 2003).

Uncertainty in rBC mass measurement (i.e., mIE_{rBC}), associated with the accuracy of selecting a known mass of Regal Black for calibration and counting the total number of particles, is ±20%. Uncertainty in mIE_{NR-PM} (RIE_{NR-PM}), based on mIE_{rBC}, is ±50%. Previous measurements of laboratory generated particles and ambient aerosol has suggested that RIE_{NR-PM} could be overestimated by up to a factor of two, resulting in an approximately 50% overestimation in NR-PM mass for hydrocarbon-like organic aerosol (HOA) species (Lee et al., 2015; Willis et al., 2014). This overestimation in NR-PM and resulting underestimation in the mass fraction of rBC (mf_{BC}) could arise due to (1) an increased sensitivity to NR-PM evaporating from rBC in the laser vaporiser and/or (2) incomplete vaporisation of rBC-containing particles in the edges of the laser vaporiser such that NR-PM is overestimated relative to rBC. A report of incomplete vaporisation for diesel engine exhaust was presented at the 16^{th} AMS Users' Meeting (http://cires1.colorado.edu/jimenezgroup/UsrMtgs/UsersMtg16/JDASPAMSfocusing.pdf), demonstrating that the effective beam width for organic species and rBC in these fractal particles can be substantially different. Both of these uncertainties in quantification of NR-PM on rBC could lead to underestimation of mf_{BC} such that values reported here should be regarded as a lower limit. Figure 3a and c of the main text shows histograms of mf_{BC} for the "standard" RIE_{NR-PM} (i.e., 1.4, shown as solid bars) and calculated by decreasing HOA mass by 50% (dashed lines). For the roadside study, these assumptions increase average mf_{BC} in rBC-rich particles from 0.86 to 0.92, and from 0.02 to 0.03 in HOA-rich particles. Further uncertainties in absolute rBC mass measurement and mf_{BC} arise from the attribution of "refractory CO_x^+" species (i.e., CO_2^+ and CO^+ as rBC or organic species)(Corbin et al., 2014). In addition, the signal for CO^+ is conventionally estimated as equal to CO_2^+ in AMS measurements based on laboratory measurements of oxygenated organic fragmentation patterns. However, we may underestimate the CO^+:C_3^+ ratio since this assumption may not be accurate for SP-AMS measurements if CO_x^+ signals arise from oxygenated moieties on the black carbon surface. Attribution of CO_x^+ signals has minimal impact on our results, as shown in Figure 3b and d of the main text, where the fraction of total BC (HOA) from BC-rich (HOA-rich) particles is shown assuming CO_x^+ species are either exclusively organic (solid bars) or rBC (dashed purple lines). CO_x^+ signals are conventionally removed from single particle data, due to air interferences in the unit mass resolution spectra, so a similar calculation was not possible in Figure 3a and c of the main text. Further characterization SP-AMS rBC and NR-PM quantification is required to reduce these uncertainties.

Collection efficiency (CE) for rBC-containing particles detected in the SP-AMS is determined by the extent of particle beam - laser beam overlap, or the fraction of particles crossing the IR-laser beam (Willis et al., 2014). CE for rBC-containing particles was determined in the roadside study using beam width probe measurements described in Willis

et al. (2014). Ambient rBC-containing particles had an average beam width $\sigma = 0.46 \pm 0.03$ mm, which is close to, but wider than that of 300 nm Regal Black particles ($\sigma = 0.40 \pm 0.08$) used for calibration (Willis et al., 2014). Ideal absolute quantification of rBC would involve a time dependent CE either from more highly time resolved measurements of particle beam width, or from comparison with rBC coating thickness derived from a single particle soot photometer (SP2), neither of which were available here. Previous work has suggested that the collection effiency for rBC and associated coating species is similar (i.e., the same CE can be applied) (Willis et al., 2014). However, other recent work noted above has suggested that the effective beam width for rBC and NR-PM can differ substantially. In this work, a constant collection efficiency of 0.6 was applied for absolute quantification of rBC and associated species. SP-AMS rBC mass loadings (both denuded and ambient) correlated well ($R^2 > 0.90$) with absorption measurements (781 nm) from a co-located photoacoustic soot spectrometer (PASS-3, Droplet Measurement Techniques, Boulder, CO) (Healy et al., 2015), suggesting that the CE did not vary dramatically during the roadside study. Note that the CE applied will not impact calculations of mf_{rBC}.

S2 Positive matrix factorization (PMF) of ensemble measurements - Roadside study

Positive matrix factorization (PMF) was performed on the one-minute time resolution SP-AMS ensemble data to determine the sources of rBC and organic aerosol sampled in the roadside study. The bilinear model was solved using the PMF2 algorithm developed by P. Paatero (Paatero and Tapper, 1994; Paatero, 2007), in robust mode, and a four-factor solution was selected using an Igor Pro (v. 6.36, WaveMetrics, Inc.) based evaluation tool (v.2.04) according to the method described by Ulbrich et al. (2009) and Zhang et al. (2011). Time series and mass spectra of the four PMF factors are presented in Figure 5 of the main text and S1. A four-factor solution was selected as appropriate for this data set based on examination of the PMF quality of fit parameter ($Q/Q_{expected}$) as a function of the number of PMF factors (Figure S2), and by examining the solutions for up to eight PMF factors. The two, three and five-factor solutions are shown in Figure S3, S4 and S5. Two factors allowed the separation of local/fresh emissions from more aged/transported aerosol. Three factors allowed the separation of biomass burning organic aerosol (BBOA) from a background oxygenated organic aerosol (OOA). Increasing the number of factors from three to four allowed for the separation of HOA-rich and rBC-rich factors, the physical meaning of which is supported by the observation of HOA-rich and rBC-rich particle classes from single particle measurements. Moving beyond four factors, splitting and/or mixing of BBOA and OOA factors became evident, so solutions with more than four factors were not considered.

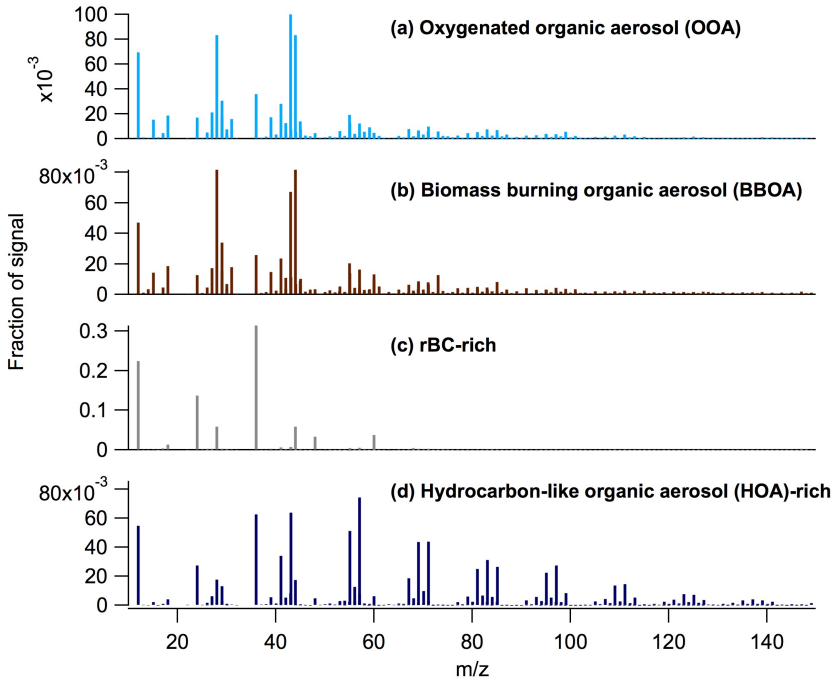


Figure S1: Ensemble data: Mass spectra of the four-factor PMF solution. The four factors represent (a) background oxygenated organic aerosol (OOA), (b) biomass burning organic aerosol (BBOA), (c) rBC-rich particles, and (d) hydrocarbon-like organic aerosol (HOA) rich particles.

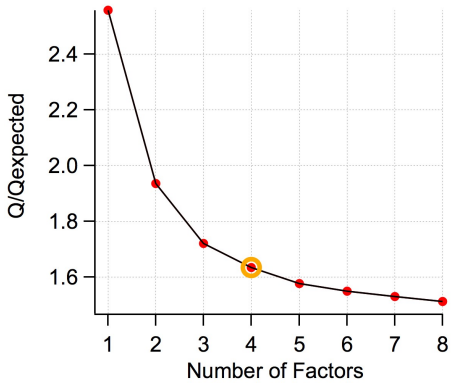


Figure S2: The PMF quality of fit parameter ($Q/Q_{expected}$) as a function of the number of factors.

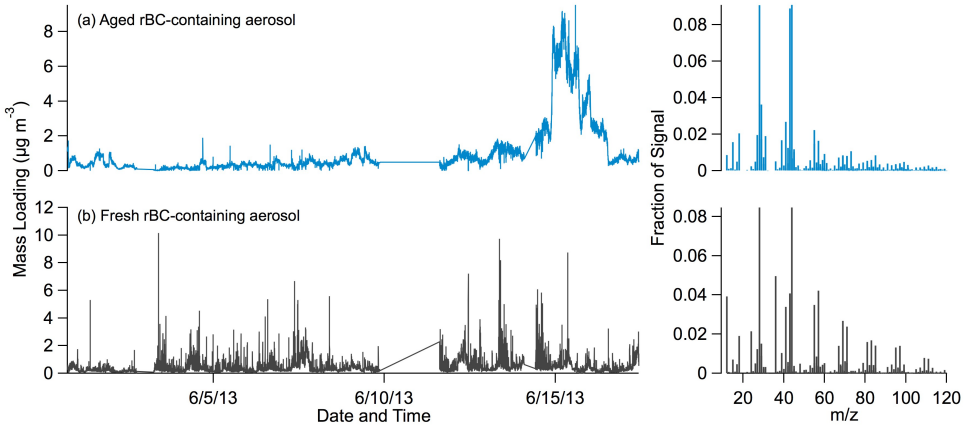


Figure S3: Time series and mass spectra corresponding to the two - factor PMF solution. rBC and organic mass loadings are represented here as nitrate equivalent mass.

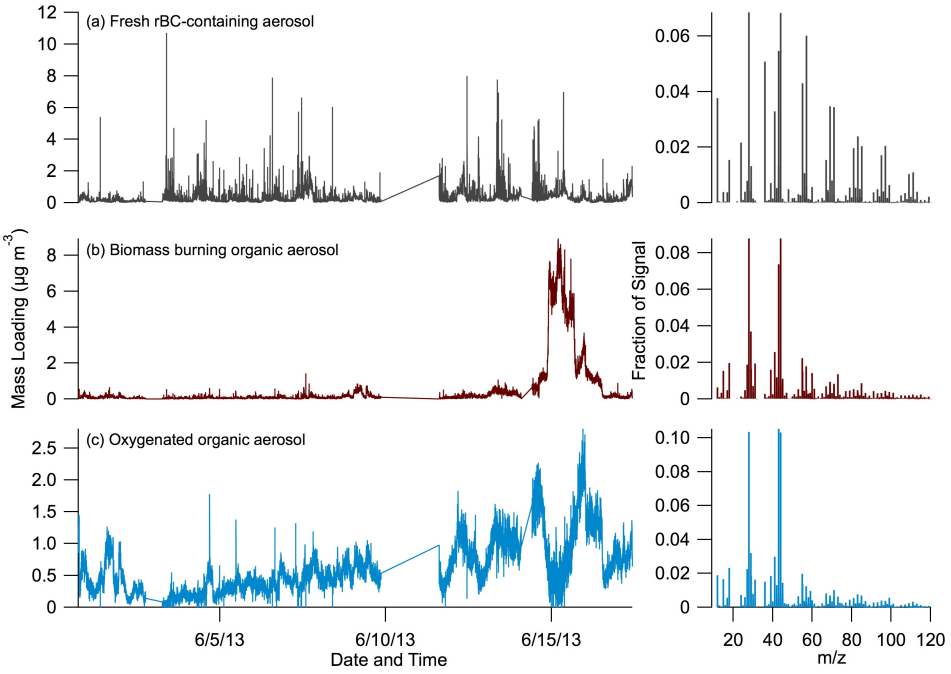


Figure S4: Time series and mass spectra corresponding to the three - factor PMF solution. rBC and organic mass loadings are represented here as nitrate equivalent mass.

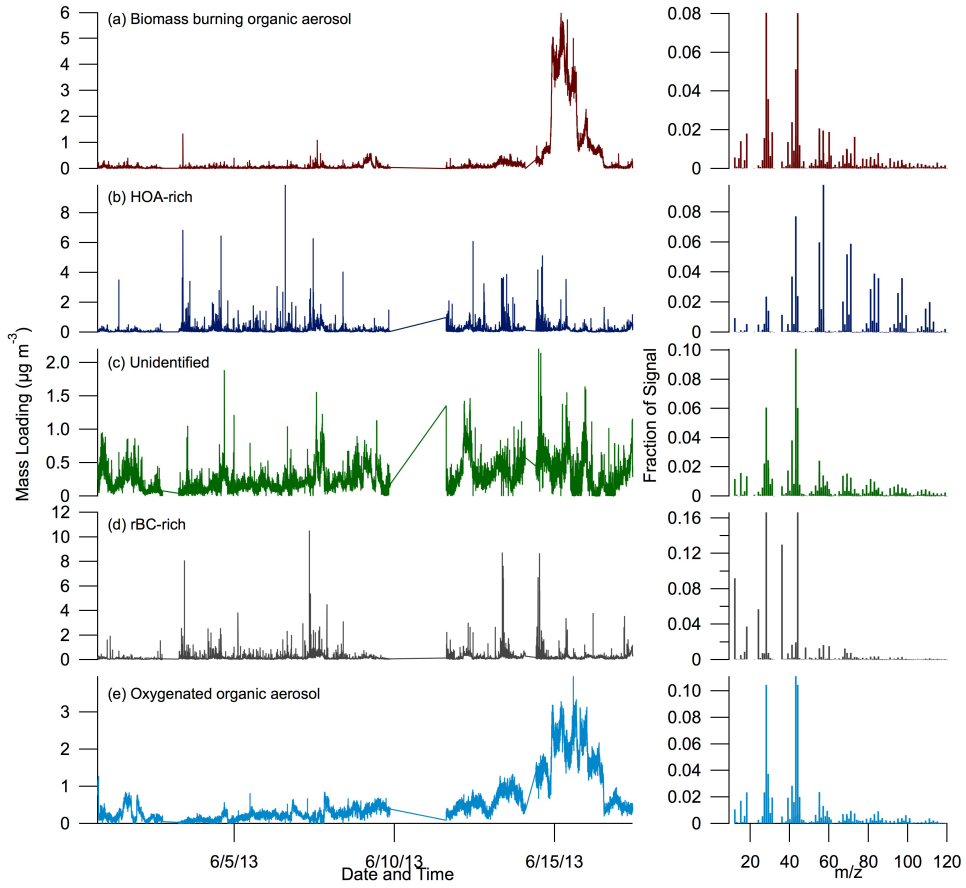


Figure S5: Time series and mass spectra corresponding to the five - factor PMF solution. rBC and organic mass loadings are represented here as nitrate equivalent mass.

S3 Determination of PartMC-MOSAIC model input parameters

S3.1 Step 1: Determine the mass-based ensemble size distributions of rBC and HOA from fresh traffic emissions

Figure S6 shows the size distributions of rBC and organic excluding periods with a strong influence from biomass burning. The size distributions were fitted with three log-normal distributions with maximum D_{va} at 96.0 (peak 1), 173.4 (peak 2) and 390.8 nm (peak 3) for both rBC and organics using the multi-peak fitting package in IGOR Pro version 6.36 (WaveMetrics, Inc.). Assuming peak 3 for both rBC and organics represents aged particles in the accumulation mode, Peaks 1 and 2 are used to represent the size distributions of the rBC and HOA originating from fresh traffic emissions.

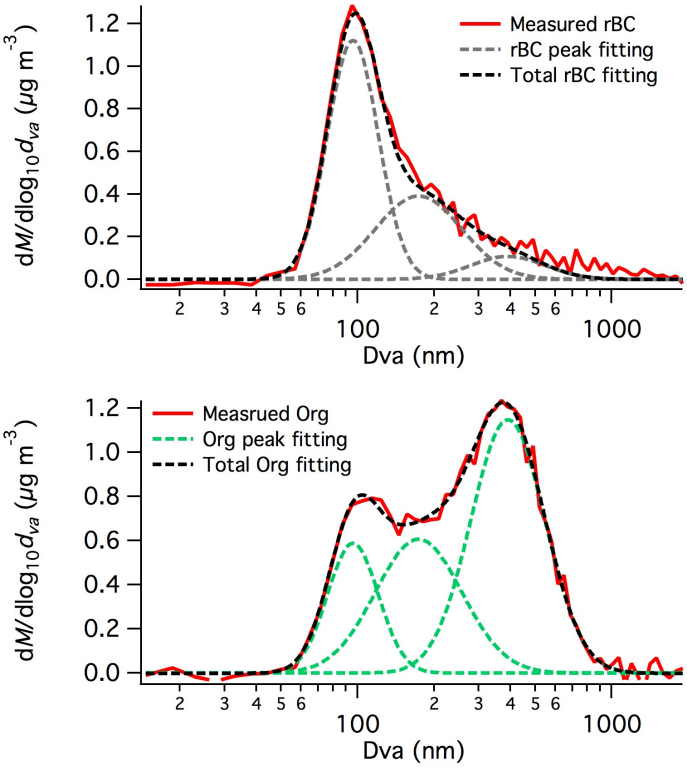


Figure S6: Size distributions of rBC (top) and organic (bottom) excluding the strong biomass burning event (red lines). The dashed lines represent the peak fitting results.

S3.2 Step 2: Determine the mass-based ensemble size distributions of rBC in rBC-rich and HOA-rich particle types

According to Figure 3d in the main text, rBC-rich and HOA-rich particle types accounted for approximately 93% and 7% of the total rBC mass, respectively. The contribution of rBC-rich and HOA-rich particle types to the total rBC mass in peak 1 and 2 can be calculated using Eq. 1 and 2, respectively. The calculation results are shown in Figure S7.

$$\mathrm{rBC}_{(\mathrm{Peaki,rBC-rich})} = \mathrm{rBC}_{(\mathrm{Peaki,total})} \cdot 0.93 \tag{1}$$

$$\mathrm{rBC}_{(\mathrm{Peaki,HOA-rich})} = \mathrm{rBC}_{(\mathrm{Peaki,total})} \cdot 0.07 \tag{2}$$

where i is the peak number from step 1 (i.e. D_{va} at 96.0 nm = peak 1 and 173.4 nm = peak 2).

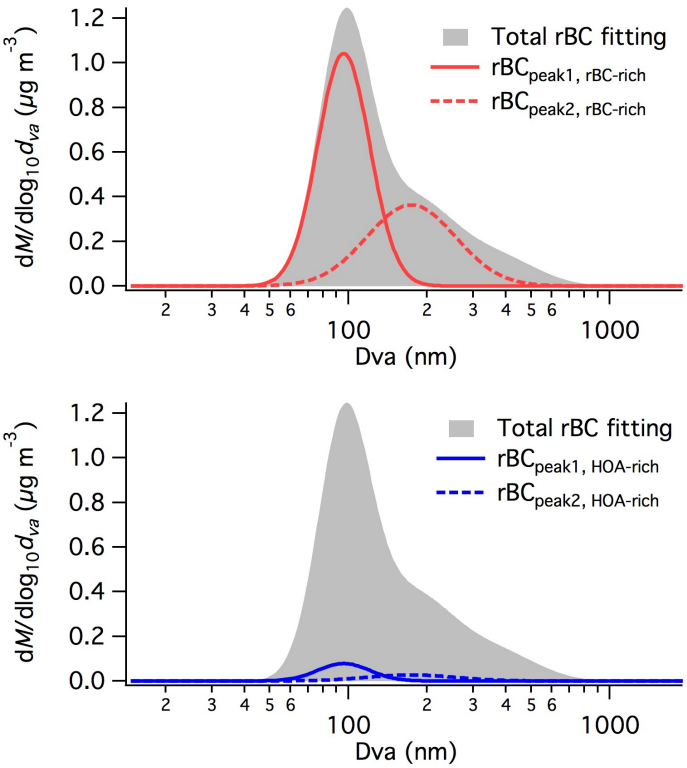


Figure S7: Size distributions of rBC in rBC-rich (top) and HOA-rich (bottom) particle types. The accumulation mode particles (i.e. peak 3 identified in step 1) are excluded in the calculation.

S3.3 Step 3: Determine the mass-based ensemble size distributions of HOA in rBC-rich and HOA-rich particle types

According to Figure 3c in the main text, rBC accounted for about 86% of total mass in the rBC-rich particles. The mass of HOA materials in rBC-rich and HOA-rich particle types in peak 1 and 2 can be calculated using Eq. 3 and 4, respectively. The calculation results are shown in Figure S8.

$$\mathrm{HOA}_{(\mathrm{Peaki,rBC-rich})} = \frac{\mathrm{rBC}_{(\mathrm{Peaki,rBC-rich})}}{0.86} \cdot 0.14 \tag{3}$$

$$\mathrm{HOA}_{(\mathrm{Peaki,HOA-rich})} = \mathrm{HOA}_{(\mathrm{Peaki,total})} - \mathrm{HOA}_{(\mathrm{Peaki,rBC-rich})} \tag{4}$$

where i is the peak number from step 1 (i.e. D_{va} at 96.0 nm = peak 1 and 173.4 nm = peak 2)

S3.4 Step 4: Determine the mass-based ensemble size distributions of rBC-rich and HOA-rich particle types

The total size distributions of rBC-rich and HOA-rich particle classes can be calculated using Eq. 5 and 6 (i.e. summation of the rBC and HOA mass in each particle type). The calculation results are shown in Figure S9.

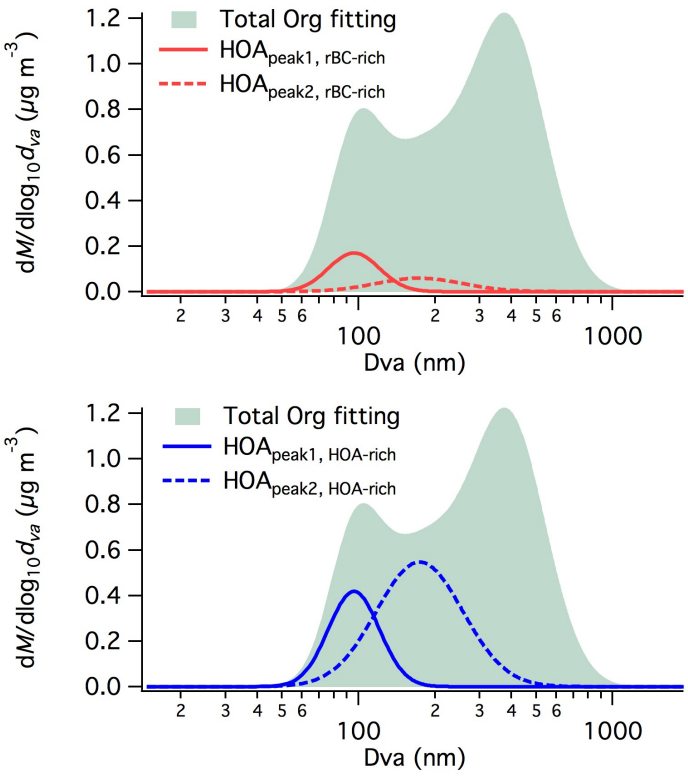


Figure S8: Size distributions of HOA in rBC-rich (top) and HOA-rich (bottom) particle types. The accumulation mode particles (i.e. peak 3 identified in step 1) are excluded in the calculation.

$$\text{Total}_{(\text{Peaki,rBC-rich})} = \text{rBC}_{(\text{Peaki,rBC-rich})} + \text{HOA}_{(\text{Peaki,rBC-rich})} \tag{5}$$

$$\text{Total}_{(\text{Peaki,HOA-rich})} = \text{rBC}_{(\text{Peaki,HOA-rich})} + \text{HOA}_{(\text{Peaki,HOA-rich})} \tag{6}$$

where i is the peak number from step 1 (i.e. D_{va} at 96.0 nm = peak 1 and 173.4 nm = peak 2)

S3.5 Step 5: Calculate the number-based size distribution parameters as model inputs

The mass-based geometric diameter and geometric standard deviation of each peak for both rBC-rich and HOA-rich particle types are calculated based on the lognormal fitting parameters obtained from Steps 2 to 4 using IGOR Pro. After that, the mass-based geometric diameter can be transformed to the number-based geometric diameter using Eq. 7 (Seinfeld and Pandis, 2006). Note that the geometric standard deviations of mass- and number-based distributions are the same. The calculation results are shown in Table S1.

$$\ln d_{pgM} = \ln d_{pgN} + 3\ln^2\sigma_g \tag{7}$$

where d_{pgM} = particle mass − based geometric diameter
d_{pgN} = particle number − based geometric diameter
σ_g = geometric standard deviation

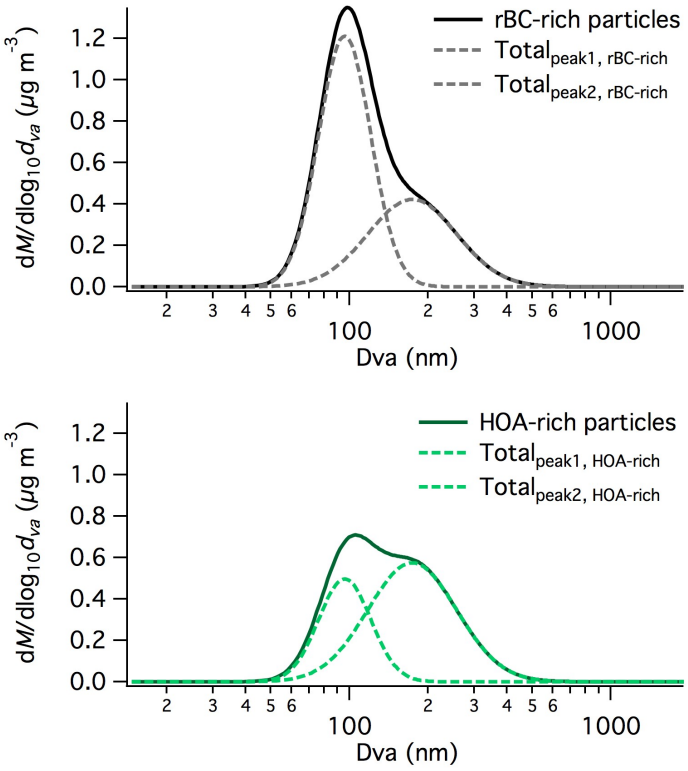


Figure S9: Size distributions of rBC-rich (top) and HOA-rich (bottom) particle types. The accumulation mode particles (i.e. peak 3 identified in step 1) are excluded in the calculation.

The mass-based (or volume-based) peak area obtained from lognormal fittings can be transformed to the number-based parameters using the following approach. The calculation results are shown in Table S1. The derived parameters can be used to constrain the ratio of rBC-rich and HOA-rich particle emission rates in the model stimulation.

The total volume (V) of a size distribution is:

$$V = \int_0^\infty n_v(d_p)d(d_p) = \int_0^\infty \frac{\pi}{6} d_p^3 n(d_p)d(d_p) \tag{8}$$

where d_p is the particle diameter. Generally, the k-th moment (M_k) of a distribution is:

$$M_k = \int_0^\infty d_p^k n(d_p)d(d_p) \tag{9}$$

The total volume is proportional to the third moment of the distribution. Combining Eq.8 and Eq. 9 and assuming spherical particles:

$$V = \frac{\pi}{6} M_3 \tag{10}$$

For a log-normal distribution, the integral for the k-th moment can be evaluated analytically:

$$M_k = \int_{-\infty}^\infty d_p^k n \cdot (lnd_p)d(lnd_p) = N d_{pg}^k \cdot e^{\frac{k^2}{2} ln\sigma_g} \tag{11}$$

The third moment of a mode is proportional to particle volume (or mass), and the particle number-based parameters (N) can be determined using Eq. 11 if d_{pg} and σ_g (geometric diameter and standard deviation of the particle number distribution) are available.

Table S1: Aerosol initial conditions and emissions for the measurement-constrained case. The symbol N denotes the total number concentration of the initial aerosol population in each log-normal mode, E is the flux of emitted particles, which is constant with time for the first 12 h of simulations and then stops, $\mathrm{mf_{BC}}$ and $\mathrm{mf_{HOA}}$ are the average values of BC and primary organic carbon mass fraction of the particles, and σ_{BC} and σ_{HOA} are the standard deviations around that mean

Quantity	**rBC-rich particles (Peak 1, BC1)**	**rBC-rich particles (Peak 2, BC2)**	**HOA-rich particles (Peak 1, HOA1)**	**HOA-rich particles (Peak 2, HOA2)**
$\mathrm{mf_{BC}}$	0.86	0.86	0.03	0.03
$\mathrm{mf_{HOA}}$	0.14	0.14	0.97	0.97
σ_{BC}	0.14	0.14	0	0
σ_{HOA}	0.14	0.14	0	0
$\mathrm{d_{pgM}}$ (nm)	101.0	202.4	101.0	202.4
σ_{g}^{*}	1.25	1.48	1.25	1.48
$\mathrm{d_{pgN}}$ (nm)*	86.7	128.6	86.7	128.6
Particle mass-based peak area from log-normal fitting	68.78	77.64	28.22	105.76
Particle number-based parameters (N) from Eq.11	1.97×10^{11}	4.35×10^{10}	7.45×10^{10}	5.38×10^{10}
N ($\mathrm{m^{-3}}$)*	1.97×10^{9}	4.35×10^{8}	7.45×10^{8}	5.38×10^{8}
E ($\mathrm{m^{-2}\,s^{-1}}$)*	2×10^{7}	4.42×10^{6}	7.56×10^{6}	5.46×10^{6}

*Data used as model input

Table S2: Aerosol initial conditions for the uniform initial mixing state case.

Quantity	Mode1	Mode2
d_{pgN} (m)	8.67	1.29
σ_{g}	1.25	1.48
N (m^{-3})	2.72×10^{9}	9.73×10^{8}
E ($\mathrm{m}^{-2}\,\mathrm{s}^{-1}$)	2.76×10^{7}	9.88×10^{6}
$\mathrm{mf}_{\mathrm{BC}}$	0.44	0.44
$\mathrm{mf}_{\mathrm{HOA}}$	0.56	0.56
σ_{BC}	0	0
σ_{HOA}	0	0

S4 Particle-resolved aerosol box model simulations

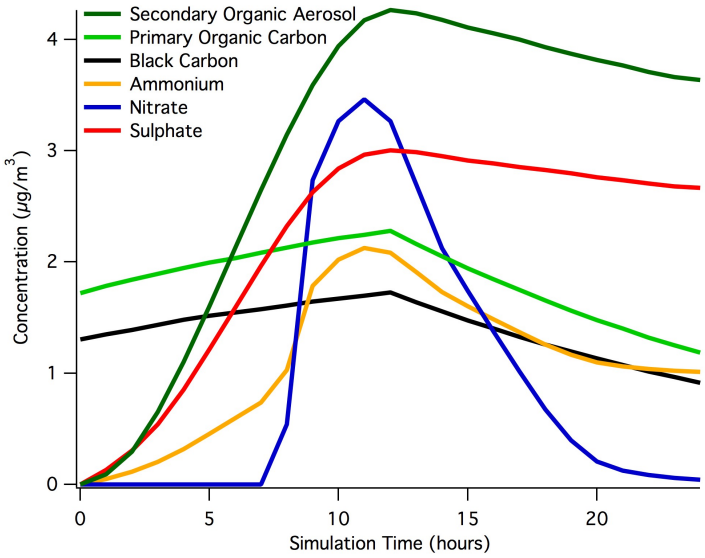


Figure S10: Mass concentrations of bulk aerosol species over the 24h simulation period in both the uniform initial and measurement constrained mixing state cases.

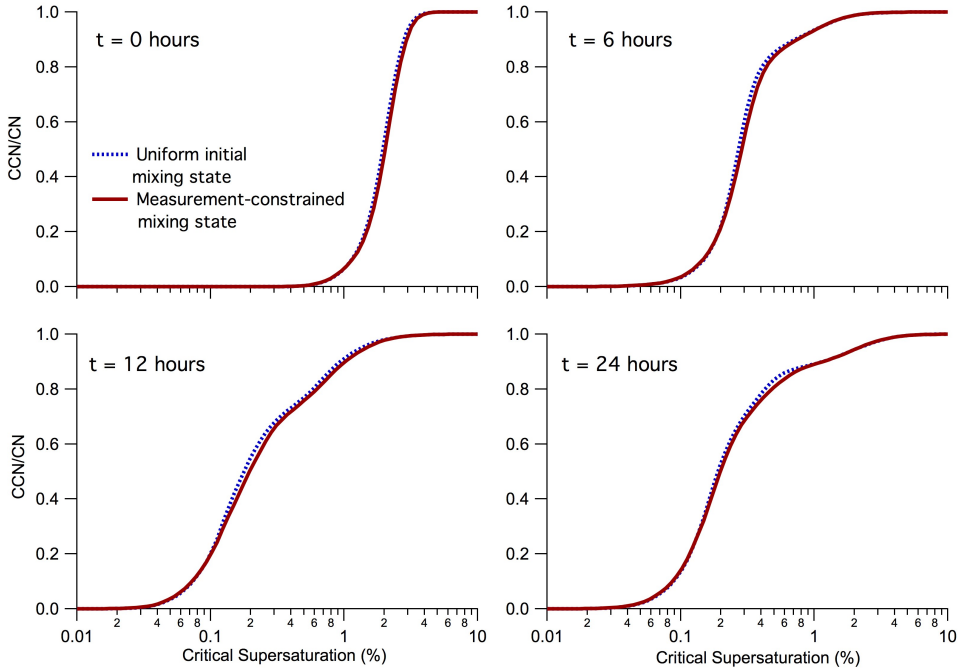


Figure S11: Modelled CCN spectra over the 24 hour simulation period for the uniform initial mixing state (dashed lines) and measurement constrained (solid lines) cases.

References

Corbin, J. C., Sierau, B., Gysel, M., Laborde, M., Keller, A., Kim, J., Petzold, A., Onasch, T. B., Lohmann, U., and Mensah, A.: Mass spectrometry of refractory black carbon particles from six sources: carbon-cluster and oxygenated ions, Atmospheric Chemistry and Physics, 14, 2591–2603, 2014.

Healy, R. M., Wang, J. M., Jeong, C.-H., Lee, A. K. Y., Willis, M. D., Jaroudi, E., Zimmerman, N., Hilker, N., Murphy, M., Eckhardt, S., Stohl, A., Abbatt, J. P. D., Wenger, J. C., and Evans, G. J.: Light-absorbing properties of ambient black carbon and brown carbon from fossil fuel and biomass burning sources, Journal of Geophysical Research: Atmospheres, 120, 6619–6633, doi:10.1002/2015JD023382, 2015.

Jimenez, J. L., Jayne, J. T., Shi, Q., Kolb, C. E., Worsnop, D. R., Yourshaw, I., Seinfeld, J. H., Flagan, R., Zhang, X., Smith, K., Morris, J., and Davidovits, P.: Ambient aerosol sampling using the Aerodyne Aerosol Mass Spectrometer, Journal of Geophysical Research-Atmospheres, 108, doi:10.1029/2001JD001213, 2003.

Lee, A. K. Y., Willis, M. D., Healy, R. M., Onasch, T. B., and Abbatt, J. P. D.: Mixing state of carbonaceous aerosol in an urban environment: Single particle characterization using a soot particle aerosol mass spectrometer (SP-AMS), Atmospheric Chemistry and Physics, 15, 1823–1841, 2015.

Onasch, T. B., Trimborn, A., Fortner, E. C., Jayne, J. T., Kok, G. L., Williams, L. R., Davidovits, P., and Worsnop, D. R.: Soot Particle Aerosol Mass Spectrometer: Development, Validation, and Initial Application, Aerosol Science and Technology, 46, 804–817, 2012.

Paatero, P.: User's guide for positive matrix factorization programs PMF2.exe and PMF3.exe, Tech. rep., University of Helsinki, Finland, 2007.

Paatero, P. and Tapper, U.: Positive matrix factorization: A non-negative factor model with optimal utilization of error estimate of data values, Environmetrics, 5, 111–126, 1994.

Seinfeld, J. H. and Pandis, S.: Atmospheric Chemistry and Physics, 2 Ed., Jon Wiley and Sons, New York, 2006.

Ulbrich, I. M., Canagaratna, M. R., Zhang, Q., Worsnop, D. R., and Jimenez, J. L.: Interpretation of organic components from Positive Matrix Factorization of aerosol mass spectrometric data, Atmospheric Chemistry and Physics, 9, 2891–2918, 2009.

Willis, M. D., Lee, A. K. Y., Onasch, T. B., Fortner, E. C., WilliamS, L. R., Lambe, A. T., Worsnop, D. R., and Abbatt, J.: Collection efficiency of the soot-particle aerosol mass spectrometer (SP-AMS) for internally mixed particulate black carbon, Atmospheric Measurement Techniques, 7, 4507–4516, 2014.

Zhang, Q., Jimenez, J. L., Canagaratna, M. R., Ulbrich, I. M., Ng, N., Worsnop, D., and Sun, Y.: Understanding atmospheric organic aerosols via factor analysis of aerosol mass spectrometry: A review, Anal. Bioanal. Chem., 401, 3045–3067, doi:10.1007/s00216-011-5355-y, 2011.